Cytometry 43:239–247 (2001)

Bioimaging

Hyperspectral Imaging: A Novel Approach For Microscopic Analysis

Roger A. Schultz,[1,2*] Thomas Nielsen,[1] Jeff R. Zavaleta,[1] Raynal Ruch,[1] Robert Wyatt,[1] and Harold R. Garner[1,3,4,5]

[1]McDermott Center for Human Growth and Development, The University of Texas Southwestern Medical Center, Dallas, Texas
[2]Department of Pathology, The University of Texas Southwestern Medical Center, Dallas, Texas
[3]Department of Biochemstry, The University of Texas Southwestern Medical Center, Dallas, Texas
[4]Department of Internal Medicine, The University of Texas Southwestern Medical Center, Dallas, Texas
[5]Center for Biomedical Inventions, The University of Texas Southwestern Medical Center, Dallas, Texas

Received 9 August 2000; Revision Received 21 November 2000; Accepted 23 November 2000

Background: The usefulness of the light microscope has been dramatically enhanced by recent developments in hardware and software. However, current technologies lack the ability to capture and analyze a high-resolution image representing a broad diversity of spectral signatures in a single-pass view. We show that hyperspectral imaging offers such a technology.

Methods and Results: We developed a prototype hyperspectral imaging microscope capable of collecting the complete emission spectrum from a microscope slide. A standard epifluorescence microscope was optically coupled to an imaging spectrograph, with output recorded by a CCD camera. Software was developed for image acquisition and computer display of resultant X–Y images with spectral information. Individual images were captured representing Y-wavelength planes, with the stage successively moved in the X direction, allowing an image cube to be constructed from the compilation of generated scan files. This prototype instrument was tested with samples relevant to cytogenetic, histologic, cell fusion, microarray scanning, and materials science applications.

Conclusions: Hyperspectral imaging microscopy permits the capture and identification of different spectral signatures present in an optical field during a single-pass evaluation, including molecules with overlapping but distinct emission spectra. This instrument can reduce dependence on custom optical filters and, in future imaging applications, should facilitate the use of new fluorophores or the simultaneous use of similar fluorophores. Cytometry 43: 239–247, 2001. © 2001 Wiley-Liss, Inc.

Key terms: light microscopy; hyperspectral imaging; fluorescence; emission spectrum; image analysis

The light microscope, first employed more than 200 years ago, offers an important tool for research and clinical applications. In recent years, basic research efforts have benefited from the development of a diversity of microscopic techniques including fluorescent analysis of probes hybridized to chromosomal DNA for gene mapping or to cellular mRNA for the in situ study of gene expression. In the clinical arena, advances in fluorescence microscopy have been valuable in fields such as immunophenotyping and clinical cytogenetics. A number of technical improvements have been critical in facilitating these new uses for the light microscope. These advances include the use of multiband pass filters to avoid image distortion, the use of better lenses, filters, and objectives with substantially reduced autofluorescence, and the development of more effective means of transmitting excitation wavelengths to an image (1,2). Moreover, the introduction of CCD cameras has offered a means to document results and capture images as digital computer files, facilitating the analysis of results with more complex probe

Grant sponsor: Texas Higher Education Coordinating Board, Applied Technology Program; Grant number: 010019-0061-1997; Grant sponsor: UT Southwestern Medical Student Research Program; Grant sponsor: Chilton Foundation; Grant sponsor: P.O'B. Montgomery Distinguished Chair.

*Correspondence to: Roger Schultz, M.D., McDermott Center for Human Growth and Development, NB10.204, The University of Texas Southwestern Medical Center, Dallas, TX 75235-8591.
E-mail: roger.schultz@email.swmed.edu

sets (3,4) and more sophisticated computer algorithms for data analysis (5–9).

Analysis of fluorophores requires an appropriate excitation wavelength to achieve an emission spectrum, with the former having a shorter wavelength and substantially higher energy. The quality of a fluorescent image generally reflects a combination of contrast and brightness. Contrast depends on the ratio of emission intensity to background light. As a consequence, the use of filters to block the excitation wavelength and prevent it from overwhelming the field is critical for providing high contrast in the detection of fluorophore emission. However, using narrow filters to restrict the background can severely limit the brightness of the fluorescent image because barrier filters allow only a portion of the actual emission spectrum to pass. Brightness is a property intrinsic to each fluorophore but also depends on illumination with the peak excitation wavelength for that fluorophore.

The compromise between contrast and brightness can be complicated further by applications designed to facilitate the evaluation of multiple fluorophores. The selection of appropriate excitation and emission filters within a single set to allow for simultaneous viewing of multiple fluorophore is quite restrictive. Commercial advances to date have produced only triple-pass combinations, one of which permits the simultaneous detection of the widely used fluorophore combination of fluorescein-5-isothiocyanate (FITC), Texas Red, and 4′,6-diamidino-2-phenylindole (DAPI; e.g., Chroma Technology Corp., www.chroma.com/data/fsc-index.cfm).

Capturing multicolored images as digital files also has technical limitations. Color CCD cameras often use filters or liquid crystals to separate red, green, and blue wavelengths onto imaging chips. The use of these cameras is restricted to resolving colors as discriminated by the filters employed. Thus, for scientific applications, the greatest sensitivity and selectivity have been achieved with black-and-white CCD cameras with optimized filters of choice. For example, Speicher et al. (4) extended fluorescence in situ hybridization (FISH) to the analysis of painting libraries representing all 24 human chromosomes, each differentially labeled with a unique combination of five fluorophore-labeled nucleotides. These complex probes were simultaneously hybridized to metaphase chromosomes, analyzed with a traditional optical filter set, and captured with a black-and-white CCD camera to identify each fluorophore. This approach is widely used (10–19) but has inherent limits in that the spectra of data are defined by the characteristics of the optical filters employed. Therefore, the system is restricted to the examination of fluorophores that can be effectively resolved from each other by filters and, as discussed above, the filters selected limit the data collected to a portion of the total emission spectrum for any one fluorophore. One alternative means for the evaluation of optical data employs the deconvolution of spectral signatures based on a two-step process involving Sagnac interferometer generation of a variable optical path difference collected by a CCD camera with subsequent analysis of the results through inverse Fourier transformation in software (20–22). However, interferometric instruments are susceptible to difficulties with image registration and lateral coherence. This technology also loses throughput because of the beam splitter design and is limited to incoherent light sources.

In addition to those fluorescence imaging approaches, a "hyperspectral image" is fully three dimensional (23), i.e., an XY spatial image at an arbitrarily large number of wavelengths. The individual signature of differing emitting bodies can be separated for a complete view. This technique was used for satellite imaging (e.g., LANDSAT; www.techexpo.com/) and more recently for detecting fluorophores in DNA sequencing (24,25) and microarray applications (H. Garner, unpublished observations). Spectral decomposition is a mathematical/algorithmic process by which individual components (e.g., emission spectra of dyes) can be uniquely separated from a composite (full spectral) image by knowing the signature of each component measured separately (e.g., dye emission spectra). Spectral decomposition is performed by using standard algorithms with code readily available (26). We describe the development of a prototype hyperspectral imaging microscope and its generality and usefulness in the capture and analysis of various images relevant to basic research and clinical diagnostic applications.

METHODS AND RESULTS

Hardware

We developed a prototype hyperspectral imaging microscope capable of collecting the complete visible emission spectrum from a microscope slide. This microscope correlates spatial and spectral information with minimal use of optical filters, offering important advantages over a standard epifluorescence microscope. The system (Fig. 1) was built around a standard Olympus IX70 epifluorescence microscope equipped with objectives such as 1.25× and 10× Plan Fluorite, 40× Plan Apochromat Dry, and 60× and 100× Plan Apochromat Oil and a set of standard filter cubes for traditional visualization of dyes through the eyepiece (Table 1). Multiple excitation sources were used, including standard 100-W mercury and xenon arc lamps, tungsten brightfield illumination, a 532-nm solid-state laser (Brimrose, Baltimore, MD), a helium neon laser (Uniphase, San Jose, CA), an argon ion laser (Uniphase), and a pulsed-doubled nitrogen dye laser (Laser Science, Inc., Franklin, MA).

The side port of the microscope was optically coupled to a SpectraPro 556i spectrograph (Acton Research Corp., Acton, MA). A narrow entrance slit into the spectrograph allowed for only one line (~0.1 μm using a 100× objective) of the image to be photographed. The spectrograph separated the polychromatic white light illuminated from this single line into its light components. Normal operation uses a grating with 50 grooves/mm and a 600-nm blaze wavelength, which allows measurement of wavelengths approximately 400–780 nm, but many different spectrograph gratings can be used for special applications and the center wavelength can be shifted under computer

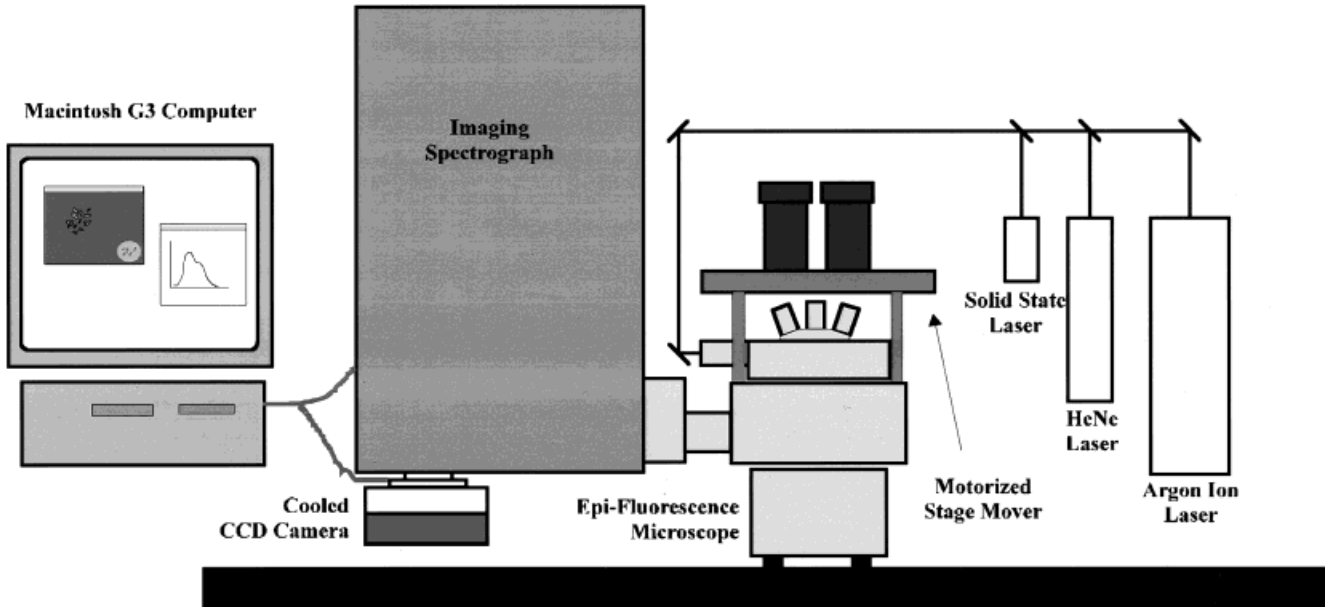

FIG. 1. Hyperspectral imaging microscope controlled with custom *Hyper*Scope software developed in house and run on a Macintosh G3 computer.

control. The output of the spectrograph was captured with a Photometrics-Synsys 1600 air-cooled CCD camera (Photometrics, Inc., Tuczon, AZ). The camera had a resolution of 1,536 × 1,024 pixels and a storage size of 12 bits/pixel. The 1,536 pixels were aligned in the spatial direction to allow the greatest spatial resolution. During normal operation, the wavelength resolution is "binned" to 128 pixels. With a sufficient number of data points to fit the emission spectrum for each fluorophore, there are adequate data to resolve approximately eight different spectra in a single excitation scan. However, higher resolution can be used for special applications.

A line of excitation light was generated with a line generator for laser excitation or a combination of slits and cylindrical lenses with traditional lamps or burners (mercury or xenon). This line of light illuminated the sample in the same position as the resulting emission light through the imaging spectrograph and onto the camera. Advantages of illumination with a line of light include decreased sample bleaching, reduced background due to scattering, and efficient use of available excitation power. A traditional bandpass or low-pass dichroic filter or a linear variable filter (Raynard Corp., San Clemente, CA) was used to select or restrict the excitation wavelength during specific applications.

The microscope was equipped with a micromover stage (Ludl) that accurately and reproducibly positioned samples to within 0.1 μ. Typically, a selected frame of interest was positioned manually or under computer control, and then the stage was incrementally moved in 0.1-μm or larger intervals during image acquisition.

Table 1
Optical Filters Used in Hyperspectral Imaging Microscopy[a]

Filter	Excitation filter	Dichromatic beam splitter	Barrier filter
U-MWU	330–385	400 LP	420 LP
U-MWIB	460–490	505 LP	515 LP
Modular	340–380	400–450	450–490
B-MAX	450–490	510–560	502–542
	533–587	590 LP	605–682
Solid-State barrier (532 nm)	NA	545	NA
He/Ne barrier (633 nm)	NA	640	NA
Argon barrier (515 nm)	NA	525	NA

[a]Values are in nanometers; LP, long pass; NA, not applicable.

Software

*Hyper*Scope, a C-language program developed in house, was written to control all hardware for acquisition and included features for analyzing and displaying the resultant X–Y images and spectral information. During a scan, individual pictures were taken in the Y-λ plane, and the stage was moved incrementally in the X direction. In this respect, the hyperspectral imaging system is distinct from all other systems designed to image visible light because wavelength is captured as a component of the two-dimensional data plane. A collection of such Y-λ scan files, generally totaling 50–1,000, were merged to build an image cube. A typical single Y-λ scan image is shown in Figure 2. Another advantage of the single-line acquisition mode is that time-dependent features can be monitored continuously. The software was designed to permit repeated collections of single lines at different times, with each image requiring 0.05 s to capture. This feature was useful because it captured images of fluorescent beads

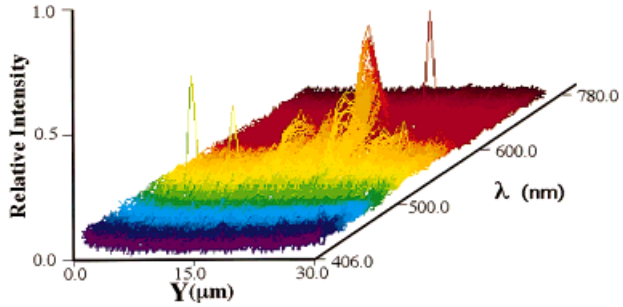

FIG. 2. A Y-λ slice from the image cube represents a single Y line (left to right) at a fixed X and all wavelengths (front to back) at each point along the Y line. As the stage motor is moved, one Y-λ image is collected for each step in the X direction. Typical image cubes are generated from 50–300 scans.

moving through an ultraviolet-transparent capillary (data not shown).

The software was designed so that the image cube would display the resultant X–Y plane. A graph of the emission spectrum for any pixel within that image could be viewed by clicking on any pixel of interest in the X–Y image. A standard linear curve fitting algorithm (26) was used to determine the contribution of individual dyes to the measured emission spectrum. The software also was designed to allow a windowing technique (integration of the emission spectra over a fixed window) that emulates standard filtering. An overlay feature within the software allowed the curve fitting results to be viewed and compared by displaying the results for multiple fluorophores in a single image. In addition, the contribution of a fluorophore was visualized by the display of a single fluorescent signature without those of others in the image or by scaling individual values up or down. Overlapping colors assigned to represent each fluorophore (by curve fitting or windowing) were viewed as added, averaged, or maximum or minimum values. For each new fluorophore–excitation source combination, the signature emission spectra were acquired and added to a library of spectra available as terms in the spectral decomposition. This enabled the user to introduce new fluorophore at any time. In addition, background spectra (defined as a region of interest by the user) could be acquired and used as one element of the decomposition. This background component could be turned off in the false color display (as could any of the spectral components), resulting in improved noise reduction and visual contrast enhancement.

Description of Acquisition

The software that controlled the microscope and performed user-directed analysis is called *Hyper*Scope. To acquire a full image, a slide was placed on the Ludl microstage mover that allowed for precise movement of the sample across the image acquisition plane. The user can position the stage with a joystick or software to move to predetermined coordinates. Focusing was done manually through a secondary optical path. The image was then scanned, with the number of scans selected at the time of each image acquisition. The sample also can be scanned at low resolution and then rescanned at a higher resolution or magnification. Each Y-λ image was saved as a single Y-λ file for each row along the sample corresponding the excitation line of light and the emission collection region that mapped through the imaging spectrograph to the CCD camera. Saving individual files allowed unlimited Y-λ image acquisition at the same Y coordinate, which is valuable for time-dependent studies. This feature also provided some robustness by permitting a partial X–Y image to be displayed if acquisition of one or more Y scans failed for any reason. After acquiring an image, the stage was moved automatically one step in the X direction to acquire emissions at the next line and generation of a second Y-λ file. Therefore, only the fluorescent probes in a line at a single X location were examined at any particular time. The minimum step size of the microstage motor, 0.1 μm, was used for scans with the 100× objective and ensured that the resolution of the device was not limited in the direction of movement. Larger step sizes were used for lower-power objectives to speed acquisition time, or when lower-resolution images were desired.

The resolution in the X direction of our images was a combination of the camera pixel size, binning in the X direction, and the microscope objective power. The camera pixel size was 9 × 9 μm and all the images had 2 pixels binned in the X direction. For a 100× object, the resolution of a displayed image was 0.18 μm per image pixel in the X direction. The resolution in the Y direction was a combination of the spectrometer entrance slit width, step size of the motorized microscope stage, number of steps moved between scans, and objective power of the microscope. The step size of the motorized stage was 0.2 μm. For a 100× objective, the software moved the stage one step per scan, or 0.2 μm per scan. For a 40μm spectrometer entrance slit width and 100× objective, the Y resolution was be 0.4 μm with some overlap of adjacent scans.

After a variable number of rows of associated emissions were captured (typically 50–1,000 scans), an image cube was loaded into memory from all the Y-λ data files. A graph of the spectrum from approximately 400–780 nm for any pixel (or bin) in the X–Y plane can be viewed in a separate window by clicking on the cube. A typical scan of 250 Y-λ files, used to construct a 250 × 1,536 × 128 (× 12 bit) image cube, consisted of approximately 100 Mb of information. Scanning an image of this size and curve fit and assigning pseudocolors took approximately 5 min on a 200-MHz G3 PowerPC Macintosh with 160 Mb of RAM.

Applications

The prototype hyperspectral imaging instrument was tested with a range of samples relevant to cytogenetic, histologic, FISH, cell fusion, microarray scanning, and materials science applications. Scanning without a fluorescent sample and barrier filters detected significant light by the camera, a result consistent with an abundance of reflected excitation wavelengths. Excitation using a standard Olympus xenon source for illumination resulted in

detection of a broad spectrum of wavelengths. A linear variable filter, 1 × 2.25 inches, coated so that light from approximately 400 to 800 nm continuously changes along its length, modulated the excitation wavelength with the xenon source. In conjunction with a slit bearing a defined width of 0.2 mm, excitation was reduced to a manually regulated 20nm bandwidth. As expected, the capture and analysis of Y-λ files showed that the wavelengths detected corresponded only to those used for excitation (data not shown). Similarly, solid-state, HeNe. and argon lasers produced emission wavelengths consistent with the sources. However, this reflected background signal could be eliminated with appropriately selected barrier filters. Therefore, to minimize such background signals and permit documentation of the unique features for hyperspectral imaging, broad-pass ultraviolet excitation and emission, multipass, or standard barrier filters were used in all subsequent applications (Table 1).

We expected hyperspectral imaging to microscopically discriminate multiple colors within a single-pass image, and it did so with multiple, differentially colored fluorescent calibration-standard microspheres (Duke Scientific Corp., Palo Alto, CA). Blue, green, and red spheres (~1 μm) were individually scanned (300 Y-λ files each) to generate files of known standards. Scanning was performed using the xenon source for excitation and the U-MWU broad-pass excitation/emission filter to restrict background fluorescence (Table 1). Subsequently, a mixture of the three colored microspheres was scanned and analyzed with the same U-MWU broad-pass excitation/emission filter and xenon source. Analysis of the resulting three-dimensional data cube for all wavelengths of 406–780 nm produced the black-and-white X–Y image shown in Figure 3. Analysis of this data cube with the three previously acquired standards (blue, green, and red spheres) produced the images in Figure 3-2 and the composite image in Figure 3-3. All fluorescent images detected in the initial analysis (406 and 780 nm) were from blue (479-nm peak), green (514-nm peak), or red (572-nm peak) microspheres. Moreover, although some beads appeared as clusters within the limits of resolution of the image analyzed, no single bead appeared to be associated with more than one microsphere standard.

FISH is a biological technique that can benefit from the resolution of many fluorophores in a single image. The three fluorophores used most often in simple FISH applications are FITC, Texas Red, and DAPI. A single triple-pass filter set to incorporate excitation and emission barriers and an appropriate dichroic mirror has been used widely in the analysis of FISH results employing these fluorophores. We expected hyperspectral imaging to acquire and decipher all three wavelengths, including multiple wavelengths at a single location. To document this utility, metaphase chromosome spreads were prepared from cells that had been synchronized and grown with 5′-bromodeoxyuridine (BrdU) only during late S phase. Incorporation during this phase of the cell cycle has been restricted principally to chromosomal G bands (27). These metaphase chromosomes were hybridized with biotinylated DNA representing the unique YAC clone 953h12 mapping to human chromosome 8p. Hybridization was detected with fluorescein-conjugated avidin. After probe detection, incorporation of BrdU was detected with a mouse anti-BrdU antibody (Sigma, Saint Louis, MO) and Texas Red–conjugated secondary antibody as previously described (28) (Jackson ImmunoResearch Laboratories, West Grove, PA). Chromosomes were counterstained with DAPI. Images of metaphases were captured with the hyperspectral imaging microscope equipped with the xenon source and the commercial B-MAX triple-pass filter set (Olympus). Independent images of fluorescein avidin, Texas Red–conjugated secondary antibody, and DAPI-stained nuclei were captured and used as spectral signature standards for metaphase image analysis. Results from the analysis of a representative metaphase are shown in Figure 4. All three fluorescent signatures in the image were identified. Moreover, single locations with multiple fluorophores were readily deconvoluted to show all wavelengths.

In addition to single-pass collection of multiple fluorophores detected by eye, we expected hyperspectral imaging to resolve two spectrally overlapping fluorophores within a single image. This feature was demonstrated by imaging cells in which mitochondria were labeled with MitoTracker Orange (Molecular Probes, Eugene, OR) and nuclear DNA with BrdU; the latter was detected with a Texas Red–conjugated secondary antibody. The emission peaks for MitoTracker Orange and Texas Red were 576 nm and 615 nm, respectively. This 39-nm difference was sufficiently large to discriminate by eye but sufficiently overlapping to limit the combined use of these fluorophores in biological applications (Fig. 5A). Double-labeled cells were analyzed using hyperspectral imaging with excitation from the xenon source and the B-MAX triple-pass filter to restrict background. Hyperscope software determined the contribution of Texas Red and MitoTracker Orange at each location on the slide and the resulting contributions were pseudocolored to facilitate visual presentation (Fig. 5B). The contribution of each fluorophore was readily discriminated. Further, consistent with the biological aspects of the experiment, Texas Red was found only in the nucleus (BrdU incorporated into nuclear DNA), whereas MitoTracker Orange was found throughout the cytoplasm (mitochondria).

Given that the prototype hyperspectral imaging microscope could resolve wavelengths of 406–780 nm, applications should analyze biological materials stained with visible dyes detectable after illumination with white light. To demonstrate this capability, tissue specimens stained with dyes typically used in histopathology were analyzed. A slide with a section of human heart mitral valve stained with hematoxylin and eosin was analyzed without filters and with standard Olympus 12-V/100-W halogen-bulb illumination. Analysis of tissue stained with hematoxylin or eosin provided the standard files necessary for deciphering the section stained with both. Figure 6A and B shows that hyperspectral imaging identified the contribution of each dye in the single-pass image. A pseudocolored dis-

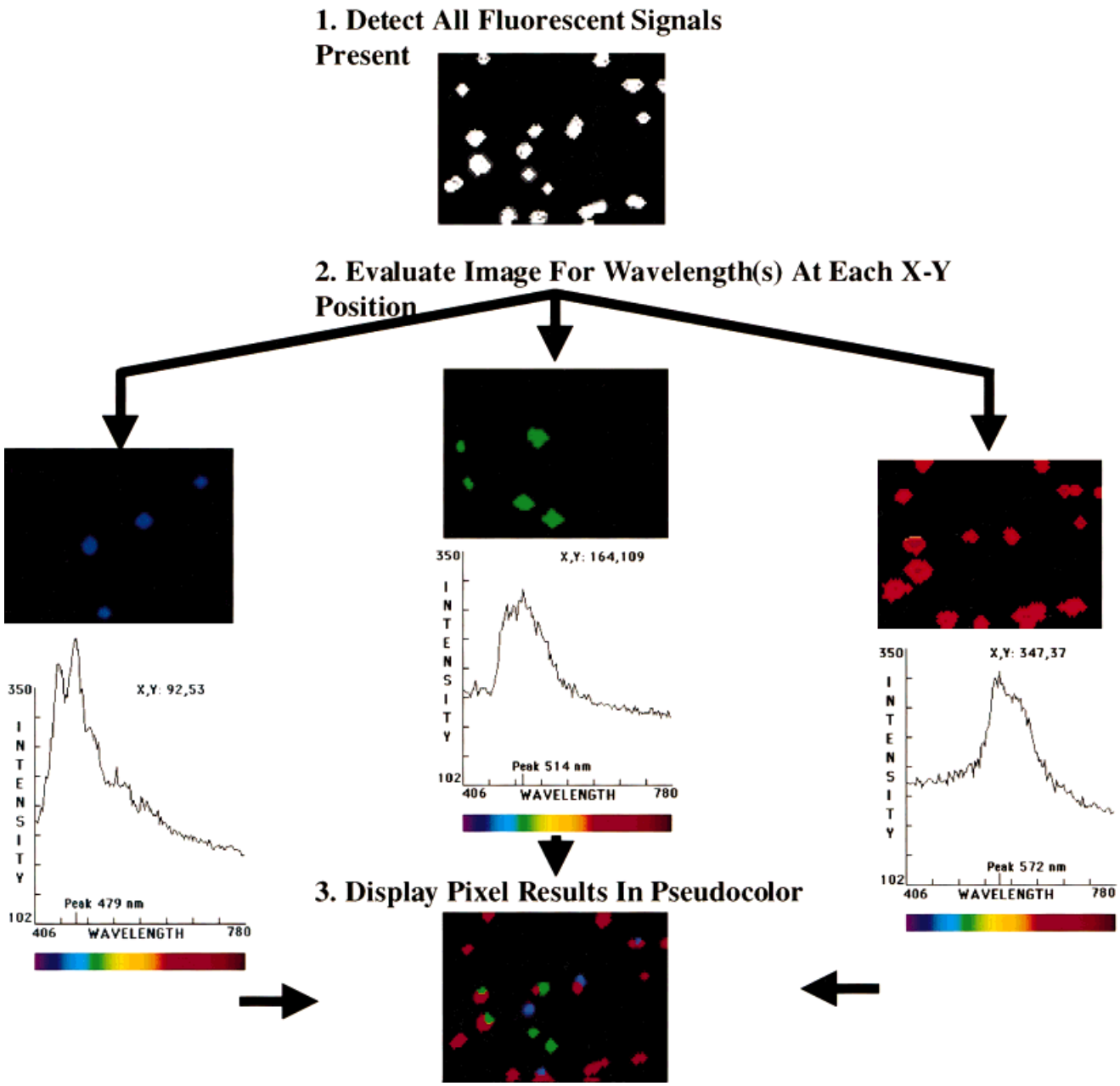

FIG. 3. Capture and analysis of multiple, differentially colored microspheres in a single-pass image. Blue, green, and red microspheres were viewed through eye pieces using the U-MWU broad ultraviolet band-pass filter cube, and an image was captured and analyzed. **1:** The initial X–Y image analyzed for all wavelengths shows all fluorescences. **2:** *Hyper*Scope software evaluated emission spectrum of each pixel on the X–Y image. The graphs show the observed emission spectra for the different colored beads at different coordinates on a slide. **3:** *Hyper*Scope was used to fit the emission spectra to standard curves to determine the fluorescent contributions at each point on the slide. Pseudocolored images were produced for analysis.

play of the composite contribution also is shown, which is comparable to that seen by eye in standard hematoxylin and eosin staining (Fig. 6C). Similar results were obtained for the analysis of a thioflavin S–stained neuropathologic cortical section (Fig. 6D).

DISCUSSION

Current fluorescent microscopy technology is limited in its ability to distinguish dyes of similar emission spectra. Many dyes whose spectra are sufficiently different can be separated by judicious use of optical filters. However, because many dyes have overlapping emission spectra, the investigator is limited in the number of dyes that can used in one sample and the quality of the final data might be compromised by the considerable spectral spillover of light from one dye into the detection channel of another. We wanted to develop a hyperspectral imaging acquisition system capable of recording the entire emission spec-

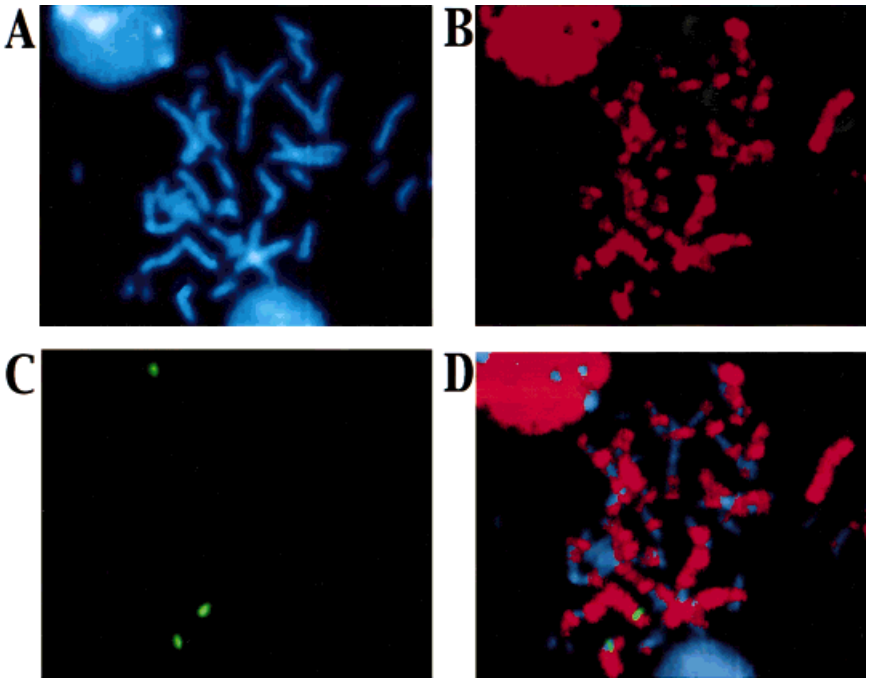

FIG. 4. Fluorescence in situ hybridization with hyperspectral imaging microscopy. The X–Y images represent analyses of image cubes collected as 300 Y-λ files with modular B-MAX (4′,6-diamidino-2-phenylindole, DAPI) or U-WIB (Texas Red and fluorescein-5-isothiocyanate) filter cubes. **A:** Metaphase chromosome spreads were generated and counterstained with DAPI (blue). **B:** The metaphase spreads have chromosomes in which 5′-bromodeoxyuridine (BrdU) was incorporated during late S phase and detected with an anti-BrdU primary antibody (Sigma) and a Texas Red–labeled anti-mouse secondary antibody (red). **C:** DNA from YAC clone 953h12 was biotinylated, hybridized to metaphase chromosomes, and detected with fluorescein avidin (yellow). **D:** A composite image was generated in which all three fluorophore results are presented in a single overlay.

trum for each pixel in a scanned image illuminated by a continuously variable excitation system. The software curve fitted each pixel in a scanned image to a user-defined set of standard dye emission spectra. Each pixel could then be assigned its own arbitrary color whose intensity depended on how well that pixel fit a specific dye emission standard.

This system allowed the separation of dyes with overlapping emission spectra and the investigator to eliminate from the display certain dyes in a sample with the click of a mouse button. The ability to identify fluorophores with overlapping spectra was demonstrated for MitoTracker Orange and Texas Red (576 nm and 615 nm, respectively; Fig. 5). Given the ability of hyperspectral imaging to detect all wavelengths in the X–Y plane, future applications will include the analysis of multiple, modestly overlapping fluorophores.

This hyperspectral imaging microscopy system is most similar to Fourier-transform imaging spectroscopy (20–22). In both cases, a continuum of spectra are taken, but there are substantial differences between hyperspectral imaging and Fourier-transform imaging spectroscopy. For the commercially available Fourier-transform spectral karyotype (SKY) instrument, deconvolution is based on two steps: collection of light passed by the filter with a Sagnac interferometer followed by an inverse Fourier transform with software. Analysis depends on the shape of a bandpass filter used for software analysis and is limited to dye sets with custom filters. As a result, photons outside the bandpass of the filter set are excluded from analysis,

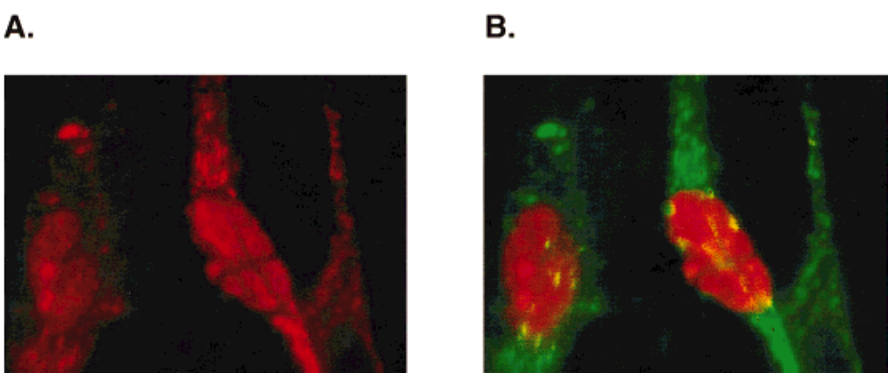

FIG. 5. Analysis with hyperspectral imaging technology allows dyes with overlapping emission peaks to be easily distinguished. Each point in this image was fit to standard emission curves for the dyes used, and the results are displayed in pseudocolor. Fibroblast mitochondria were labeled with MitoTracker Orange (Molecular Probes), and 5′-bromodeoxyuridine incorporated into nuclear DNA was detected with a Texas Red–labeled secondary antibody. **A:** Images photographed on 35-mm film show that, as viewed by eye, two fluorophore with emission peaks differing by only ~30 nm are difficult to resolve. **B:** In contrast, images captured by hyperspectral imaging can be analyzed with routine curve-fitting software to determine the contributions of both fluorophores at each pixel. Results are shown in pseudocolor (red: Texas Red; green: MitoTracker Orange), facilitating visual localization of each fluorophore.

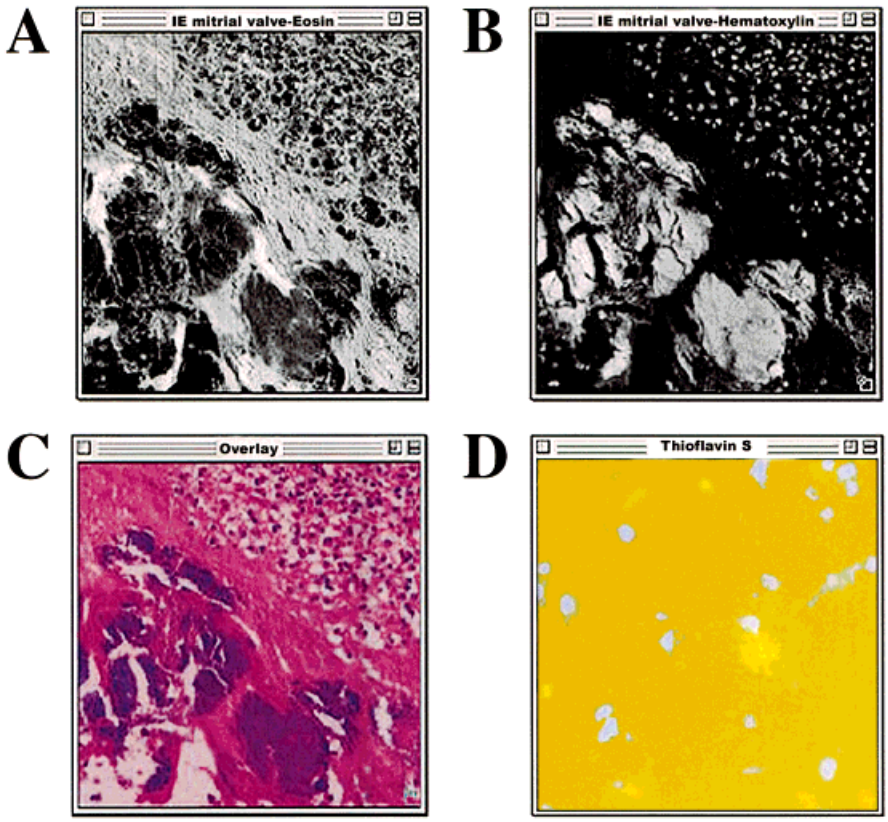

FIG. 6. Hyperspectral imaging microscopy to analyze traditional brightfield stains. The images show standard eosin- (**A**) and hematoxylin- (**B**) stained pathologic sections of a human mitral valve for an evaluation of the contribution of each dye to the field. **C:** A pseudocolored composite image of A and B. **D:** Different aspects of an acquired spectrum are highlighted for a neuropathologic cortical section stained with thioflavin S. The yellow plaque clearly visible in D was not be seen when the section was examined by eye on the microscope.

with a reduction in sensitivity. Of more general interest, interferometry is susceptible to image registration and lateral coherence difficulties (29) (T. B. Anderson, SAIC, Inc., personal communication).

The present hyperspectral imaging applications were based on our experience with other hyperspectral imaging systems and data analysis. Two other imaging spectrograph systems were constructed. The first system was integrated into the high-throughput DNA gel-based sequencer Astral (24,25). The Astral sequencer was designed with 144 lanes, eight-color detection, and sensitivity equal to or greater than state-of-the-art commercial machines, but with no moving parts. Another use of this technology was the hyperspectral microarray analysis system developed within our group. This system analyzed spotted microarrays in our facility and had a sensitivity of approximately 0.5 fluors/μ^2, which is comparable to that of commercial two-color scanners.

As demonstrated in this study, hyperspectral imaging can be applied to numerous fluorescent and brightfield applications, and its design should lend itself to specific improvements. For example, a microchannel plate amplifier (Videoscope International, Ltd.) installed between the CCD camera and the imaging spectrograph would substantially improve sensitivity (500–10,000 gain). However, because the pitch of available microchannel plate amplifiers is one-third that of current CCD cameras, there is increased sensitivity but decreased spatial and spectral resolution by a factor of approximately 3. Amplifiers with higher resolutions might rectify this loss. Another advantage of the hyperspectral imaging microscope is that the collected images reflect only the Y-λ plane, making a single line of light as the source for image illumination feasible. Therefore, a system capable of generating a line of light composed of variable or complex wavelengths could be incorporated to precisely control excitation. Such improvements in a hyperspectral imaging microscopy might provide a new technology in many clinical and basic research applications.

LITERATURE CITED

1. Piston DW. Choosing objective lenses: the importance of numerical aperture and magnification in digital optical microscopy. Biol Bull 1998;195:1–4.
2. Dunn KW, Wang E. Optical aberrations and objective choice in multicolor confocal microscopy. Biotechniques 2000;28:542–550.
3. Schrock E, duManoir S, Veldman T, Schoell B, Wienberg J, Ferguson-Smith MA, Ning Y, Ledbetter DH, Bar-Am I, Soenksen D, Garini Y, Ried T. Multicolor spectral karyotyping of human chromosomes. Science 1996;273:494–497.
4. Speicher MR, Ballard SG, Ward DC. Karyotyping human chromosomes by combinatorial multi-fluor FISH. Nat Genet 1996;12:368–375.
5. Berland K, Jacobson K, French T. Electronic cameras for low-light microscopy. Methods Cell Biol 1998;56:19–44.
6. Cardullo RA, Alm EJ. Introduction to image processing. Methods Cell Biol 1998;56:91–115.
7. Inoue T, Gliksman N. Techniques for optimizing microscopy and analysis through digital image processing. Methods Cell Biol 1998;56:63–90.

8. Wang YL. Digital deconvolution of fluorescence images for biologists. Methods Cell Biol 1998;56:305–315.
9. Boland MV, Murphy RF. Automated analysis of patterns in fluorescence-microscope images. Trends Cell Biol 1999;9:201–202.
10. Anguiano A. Fluorescence in situ hybridization (FISH): Overview and medical applications. J Clin Ligand Assay 2000;23:33–42.
11. Bezrookove V, Hansson K, van der Burg M, van der Smagt JJ, Hilhorst-Hofstee Y, Wiegant J, Beverstock GC, Raap AK, Tanke H, Breuning MH, Rosenberg C. Individuals with abnormal phenotype and normal G-banding karyotype: improvement and limitations in the diagnosis by the use of 24-colour FISH. Hum Genet 2000;106:392–398.
12. Bernheim A, Vagner-Capodano AM, Couturier J. From cytogenetics to cytogenomics of tumors. S Med Sci 2000;16:528–539.
13. Zhao L, Hayes K, Glassman A. Enhanced detection of chromosomal abnormalities with the use of RxFISH multicolor banding technique. Cancer Genet Cytogenet 2000;118:108–111.
14. Gribble SM, Roberts I, Grace C, Andrews KM, Green AR, Nacheva EP. Cytogenetics of the chronic myeloid leukemia-derived cell line K562: karyotype clarification by multicolor fluorescence in situ hybridization, comparative genomic hybridization, and locus-specific fluorescence in situ hybridization. Cancer Genet Cytogenet 2000;118:1–8.
15. Lu YJ, Morris JS, Edwards PAW, Shipley J. Evaluation of 24-color multifluor-fluorescence in-situ hybridization (M-FISH) karyotyping by comparison with reverse chromosome painting of the human breast cancer cell line T-47. Chromosome Res 2000;8:127–132.
16. Johannes C, Chudoba I, Obe G. Analysis of X-ray-induced aberrations in human chromosome 5 using high-resolution multicolour banding FISH (mBAND). Chromosome Res 1999;7:625–633.
17. Schwartz S. Molecular cytogenetics: show me the colors. Genet Med 1999;1:178–180.
18. Jalal SM, Law ME. Utility of multicolor fluorescent in situ hybridization in clinical cytogenetics. Genet Med 1999;1:181–186.
19. Raap AK. Advances in fluorescence in situ hybridization. Mutat Res Fund Mol Mech Mutag 1998;400:287–298.
20. Garini Y, Katzir N, Cabib D, Buckwald RA, Soenksen D, Malik Z. Spectral bio-imaging. In: Wang XF, Herman B, editors. Fluorescence imaging spectroscopy and microscopy. New York: John Wiley & Sons; 1996.
21. Malik Z, Cabib D, Buckwald RA, Talmi A, Garini Y, Lipson SG. Fourier transform multipixel spectroscopy for quantitative cytology. J Microsc 1996;182:133–140.
22. Garini Y, Macville, du Manoir S, Buckwald RA, Lavi M, Katzir N, Bar-Am I, Schrock E, Cabib D, Ried T. Spectral karyotyping. Bioimaging 1996;4:65–72.
23. Kruse F. The spectral image processing system (SIPS)—interactive visualization and analysis of imaging spectrometer data. Remote Sens Environ 1993;44:145–163.
24. O'Brien KM, Wren J, Dave VK, Bai D, Anderson RD, Rayner S, Evans GA, Dabiri AE, Garner HR. ASTRAL, a hyperspectral imaging DNA sequencer. Rev Sci Instrum 1998;69:2141–2146.
25. Jaklevic JM, Garner HR, Miller GA. Instrumentation for the genome project. Annu Rev Biomed Engin 1999;1:649–678.
26. Press WH, Flannery BP, Teukolsky SA, Vetterling WT. Numerical recipes, the art of scientific computing. New York: Cambridge University Press; 1986.
27. Craig CM, Bickmore WA. The distribution of CpG islands in mammalian chromosomes. Nat Genet 1994;7:376–382.
28. Tonk V, Schneider NR, Delgado MR, Mao J-i, Schultz RA. Identification and molecular confirmation of a small chromosome 10q duplication [dir dup(10)(q24.2-q24.3)] inherited from a mother mosaic for the abnormality. Am J Med Genet 1996;61:16–20.
29. Gothot A, Grosdent J, Palulus J. A strategy for multiple immunophenotyping by image cytometry: model studies using latex microbeads labeled with seven Streptaviden-bound fluorochromes. Cytometry 1996;24:214–225.